AMERICAN SOCIETY FOR MICROBIOLOGY | Journal of Virology®

STRUCTURE AND ASSEMBLY

SAT2 Foot-and-Mouth Disease Virus Structurally Modified for Increased Thermostability

Katherine A. Scott,[a,b] Abhay Kotecha,[c] Julian Seago,[d] Jingshan Ren,[c] Elizabeth E. Fry,[c] David I. Stuart,[c,e] Bryan Charleston,[d] Francois F. Maree[a,f]

Transboundary Animal Disease Programme, ARC-Onderstepoort Veterinary Institute, Onderstepoort, South Africa[a]; Department of Veterinary Tropical Diseases, Faculty of Veterinary Science, University of Pretoria, Onderstepoort, South Africa[b]; Division of Structural Biology, University of Oxford, Headington, Oxford, United Kingdom[c]; The Pirbright Institute, Pirbright, Woking, United Kingdom[d]; Life Science Division, Diamond Light Source, Harwell Science and Innovation Campus, Didcot, United Kingdom[e]; Department of Microbiology and Plant Pathology, Faculty of Agricultural and Natural Sciences, University of Pretoria, Pretoria, South Africa[f]

ABSTRACT Foot-and-mouth disease virus (FMDV), particularly strains of the O and SAT serotypes, is notoriously unstable. Consequently, vaccines derived from heat-labile SAT viruses have been linked to the induction of immunity with a poor duration and hence require more frequent vaccinations to ensure protection. *In silico* calculations predicted residue substitutions that would increase interactions at the interpentamer interface, supporting increased stability. We assessed the stability of the 18 recombinant mutant viruses in regard to their growth kinetics, antigenicity, plaque morphology, genetic stability, and temperature, ionic, and pH stability by using Thermofluor and inactivation assays in order to evaluate potential SAT2 vaccine candidates with improved stability. The most stable mutant for temperature and pH stability was the S2093Y single mutant, while other promising mutants were the E3198A, L2094V, and S2093H single mutants and the F2062Y-H2087M-H3143V triple mutant. Although the S2093Y mutant had the greatest stability, it exhibited smaller plaques, a reduced growth rate, a change in monoclonal antibody footprint, and poor genetic stability properties compared to those of the wild-type virus. However, these factors affecting production can be overcome. The addition of 1 M NaCl was found to further increase the stability of the SAT2 panel of viruses. The S2093Y and S2093H mutants were selected for future use in stabilizing SAT2 vaccines.

IMPORTANCE Foot-and-mouth disease virus (FMDV) causes a highly contagious acute vesicular disease in cloven-hoofed livestock and wildlife. The control of the disease by vaccination is essential, especially at livestock-wildlife interfaces. The instability of some serotypes, such as SAT2, affects the quality of vaccines and therefore the duration of immunity. We have shown that we can improve the stability of SAT2 viruses by mutating residues at the capsid interface through predictive modeling. This is an important finding for the potential use of such mutants in improving the stability of SAT2 vaccines in countries where FMD is endemic, which rely heavily on the maintenance of the cold chain, with potential improvement to the duration of immune responses.

KEYWORDS FMDV, SAT2, stability

Received 6 December 2016 **Accepted** 6 March 2017

Accepted manuscript posted online 15 March 2017

Citation Scott KA, Kotecha A, Seago J, Ren J, Fry EE, Stuart DI, Charleston B, Maree FF. 2017. SAT2 foot-and-mouth disease virus structurally modified for increased thermostability. J Virol 91:e02312-16. https://doi.org/10.1128/JVI.02312-16.

Editor Julie K. Pfeiffer, University of Texas Southwestern Medical Center

Address correspondence to Francois F. Maree, mareef@arc.agric.za.

Emerging and reemerging diseases caused by RNA viruses represent major threats to both public and animal health, the latter of which contributes to food insecurity. Foot-and-mouth disease virus (FMDV), an *Aphthovirus* within the family *Picornaviridae*, is a highly infectious, antigenically variable pathogen of cloven-hoofed animals. It is often difficult to control because of its high mutation rate, which leads to the emer-

gence of novel antigenic variants with the capacity to evade the immune response (1–3). The disease, characterized by fever and lesions of the mouth and hoof area, severely damages milk and meat production and draft power when it coincides with the lowing season (4–6). The most effective method of control is for countries of endemicity to embark on preventative vaccination programs.

In the developing world, FMDV is widely distributed, with unique epidemiological patterns, especially in Africa and Asia (7). In Africa, FMDV is maintained by the African buffalo (*Syncerus caffer*), in a cycle involving wildlife, and independently within domestic animals (8–11). In southern Africa, sporadic infections of livestock and wildlife with the three Southern African Territories (SAT) serotypes, i.e., SAT1, SAT2, and SAT3, with multiple topotypes (8, 12–15), readily occur from buffalo transmission (16–18). Therefore, FMD control in sub-Saharan Africa relies on regular vaccination of susceptible species in high-risk areas, fences separating animals at the wildlife-livestock interface, movement restriction, and regular surveillance (19).

In many countries where FMD is endemic, the effective administration of FMD vaccines and the optimal production of protective immunity are inadequate. This has been linked to factors including poor duration of immunity (20), vaccine potency (21), the biophysical (temperature and pH) stability of the antigen (20), and poor cross-protection due to multiple antigenic variants in these regions (22). The poor duration of immunity has been linked to the temperature lability of viruses belonging to the SAT serotypes (23). One of the foremost factors which influences the potency of vaccine preparations and permits the induction of a protective antibody response is the structural integrity of the intact virion, typified by a sedimentation rate of 146S (23). As a consequence, many countries in Africa have to rely on a triple or quadruple annual vaccination schedule.

The self-assembly and stability of a multimeric protein capsid, such as that of FMDV, depend on the occurrence of numerous noncovalent interactions between virally encoded polypeptide subunits (24–27). The icosahedral capsid of FMDV is composed of 60 repetitions of four viral structural proteins, VP1 to -4, which assemble into protomeric subunits and pentameric intermediates. Twelve pentamers self-assemble through complex protein-protein interactions into a complete capsid (28–32). Even in the presence of high genetic variability, the viral capsid intersubunit interactions for the seven serotypes are required to be sufficiently robust to provide stability to the capsid under environmental denaturing conditions (30, 31). However, the capsid still needs to be sufficiently unstable to permit intracellular uncoating and release of viral RNA during infection. The solution to this paradox in capsid metastability appears to be markedly different for different FMDV serotypes. Serotypes A and Asia-1 are relatively stable, while the O and SAT serotypes are more sensitive to heat and pH (23, 33). Additionally, chemical inactivation renders the antigens even less stable, and above 30°C, they rapidly convert into pentameric subunits which do not induce protective immune responses (23, 28, 34).

Experimental studies on the relative importance of residues and molecular interactions in viral capsid assembly, disassembly, and/or stability are still limited (26). Recent research compared the interpentamer interfaces of more thermostable serotype A viruses with those of less stable O and SAT2 viruses in the crystallographic structures of the capsids and used *in silico* calculations of stability to predict residue substitutions that may increase interactions at these interfaces (35). SAT2 and O viruses with improved stability were developed as a proof of concept (35).

This paper extends the proof of concept and describes the evaluation of the thermostability of mutants derived from the SAT2/ZIM/7/83 virus, including 14 mutants with single amino acid substitutions, 2 with triple mutations, and 2 with quadruple mutations at the interpentamer interface of the capsid. We assessed the stability of the recombinant mutant viruses in regard to the following parameters in order to evaluate potential SAT2 vaccine candidates with improved stability: growth kinetics; temperature and pH inactivation rates; results of a Thermofluor particle stability thermal release

TABLE 1 SAT2 capsid-stabilizing mutations located at or near the 2-fold axis, on the alpha-helix of the interpentamer interface[a]

Mutation(s)	ΔΔ*G* (kcal/mol)
S2093H	−5.3
S2093Y	−12.2
S2093F	−13.2
S2093W	−21.9
L2094V	−5.2
Y2098F	−5.6
S2113G	
D3193H[b]	
E3198A[b]	
F2062Y, H2087M, H3143V	−8.3
F2062Y, H2087M, Y2098F, H3143V	−4.4

[a]The change in binding free energy was calculated by including a negative control, the S2113G mutant, to validate the simulation protocol.

[b]The D3193H and E3198A mutants were not used in the simulation because both of the involved residues are near a 3-fold region of the capsid which is disordered in the crystal structure. Calculations for this region will produce ambiguous results.

assay (PaSTRY) (35) to distinguish capsid dissociation in relation to temperature, pH, and ionic strength; antigenicity; plaque morphology; and genetic stability.

RESULTS

Identification of putative mutations that confer increased SAT2 stability. Using the three-dimensional structures of FMDVs (including SAT1 [36] and SAT2 [35] viruses), we targeted residues at the interface between the pentamers for stabilization by enhancing noncovalent interactions (note that VP2 contributes the majority of the interface residues, followed by VP3). Predicted mutations were based on sequence and structural comparisons to more stable FMDV serotypes and other picornaviruses and on *in silico* calculated binding energies, but not all mutations could be simulated owing to structural disorder in the vicinity of the 3-fold axis (35) (Table 1). Mutating residues at the VP2-VP3 interface (Fig. 1A) allowed us to introduce a potentially stabilizing noncovalent interaction without disrupting viral antigenicity and infectivity. There is an alpha-helix at the pentamer interface on the 2-fold axis; triple mutants were designed to cap the dipole of this helix (31, 37), and they showed good *in silico* stability (Fig. 1B and C; Table 1). The quadruple mutants introduced additional mutations to counter clashes observed in the *in silico* molecular dynamics simulations with some mutants. Overall, combinations of stabilizing mutations did not produce additive effects in the *in silico* stability predictions, except in the case of the helix-capping mutations involving the F2062Y substitution. The infectious clone of the vaccine strain SAT2/ZIM/7/83 (38) was chosen as our target virus, and A24 Cruizero was used as a reference strain with known stability (35).

To study the effects of individual or combined mutations, we constructed recombinant virus mutants in an infectious, genome-length clone of FMDV, pSAT2 (Fig. 2). We introduced the following mutations into the VP2 coding region: F2062Y, H2087M, H2087V, Y2098H, Y2098F, S2093F, S2093Q, L2094V, T2114N, and K2215L. We also introduced the following mutations into the VP3 coding region: H3143V, D3193H, T3194A, and E3198A (Fig. 2). Two triple mutants, with the substitution combinations F2062Y-H2087M-H3143V and F2062Y-H2087V-H3143V, and quadruple mutants with the substitution combinations F2062Y-H2087V-Y2098H-H3143V and F2062Y-H2087V-Y2098F-H3143V (Fig. 2) were also constructed. Additionally, three previously described single mutants in VP2, i.e., the S2093H, S2093Y, and S2093W mutants, were included in the study (35). The VP2 S2113G mutant was selected as a negative control to validate the molecular dynamics protocol whereby a salt bridge or hydrogen bond network was deliberately disrupted; this mutation resulted in a positive ΔΔ*G* value and a destabilized interface (Table 1).

Infectivity and growth characteristics of engineered mutants. The effects of the targeted amino acid mutations on the infectivity of the SAT2 virus in susceptible cells

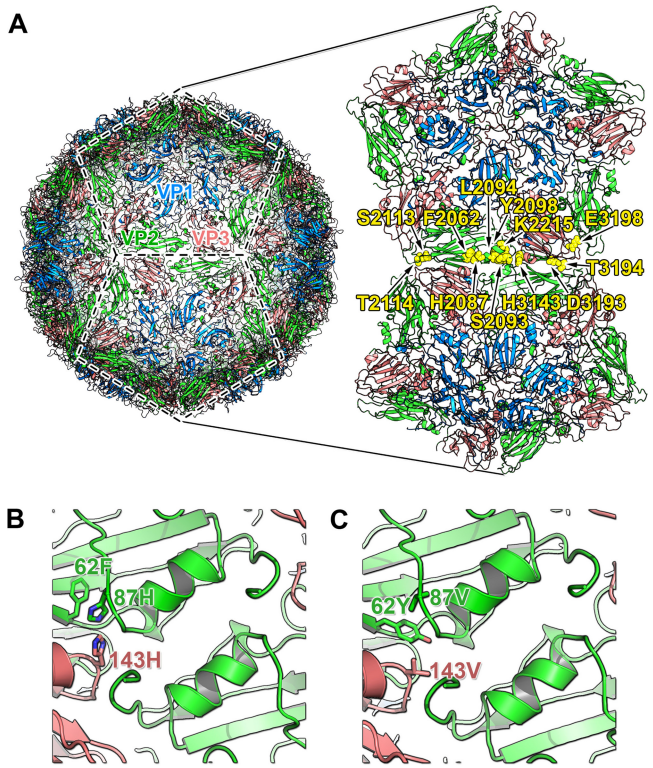

FIG 1 Stabilization of the SAT2 interpentamer interface and design of the models used for molecular dynamics simulations. (A) Cartoon representation of atomic structure of a virus capsid, with two pentameric subunits delineated and enlarged to show the interpentamer interface. The external proteins forming an icosahedral protomeric unit are labeled as follows: blue, VP1; green, VP2; and red, VP3. A truncated model was generated by trimming the protomers to include VP2 and VP3 atoms within a 13-Å radius from the interface. Yellow spheres represent amino acids interacting at the interface that were replaced in this study. Wild-type (B) and substituted (C) residues capping the 2-fold symmetry-related helix for the SAT serotype are highlighted and labeled in green for VP2 and red for VP3.

were investigated. Transcripts generated from each construct were transfected into BHK-21 cells to generate infectious FMDV stocks (passage 0 [P0] stocks). Lysates of these cells were then used to infect ZZ-R127 goat epithelium cells (P1), which are highly susceptible to FMDV infection (39). Subsequent passages were performed in BHK-21 cells. Sequencing of each mutant vSAT2 virus after four consecutive passages (P4) revealed no unintentional changes in any of the mutants and no obvious subpopulations. All viable mutant vSAT2 viruses produced a clear cytopathic effect (CPE). In the later stages of infection, cells infected with the wild-type (WT) virus exhibited large areas of cell death and loss of adherence, correlating with medium to large plaque sizes (medium, 3 to 5 mm; and large, 6 to 8 mm), whereas cells infected with the S2093Y and S2093W viruses showed numerous microscopic ($<$1 mm) foci of dead cells and plaques (Table 2). The remaining mutant viruses exhibited patterns of CPE and plaque sizes similar to those of the wild-type virus. Viruses were not recovered with the Y2098F, Y2098H, T2114N, K2215L, T3194G, F2062Y-H2087V-Y2098F-H3143V, and F2062Y-H2087V-Y2098H-H3143V mutant constructs. Viruses recovered with the S2093F, S2093Q, and F2062Y-H2087V-H3143V mutant constructs grew to very low titers (5.2×10^3 to 7.2×10^3 PFU/ml) and could not be used for further analyses.

To explore the growth properties of the wild-type and F2062Y-H2087M-H3143V, S2093H, and S2093Y mutant viruses in more detail, growth kinetics were determined in BHK-21 monolayer cells by using a starting multiplicity of infection (MOI) of 10, equivalent to 10^7 PFU/ml. The growth analysis illustrated a statistically significant ($P < 0.05$), 5-fold decrease in the virus titer of the S2093Y virus compared to that of the WT virus at 24 h postinfection (h.p.i.) and a 10-fold decrease at 12 h.p.i. In addition, the

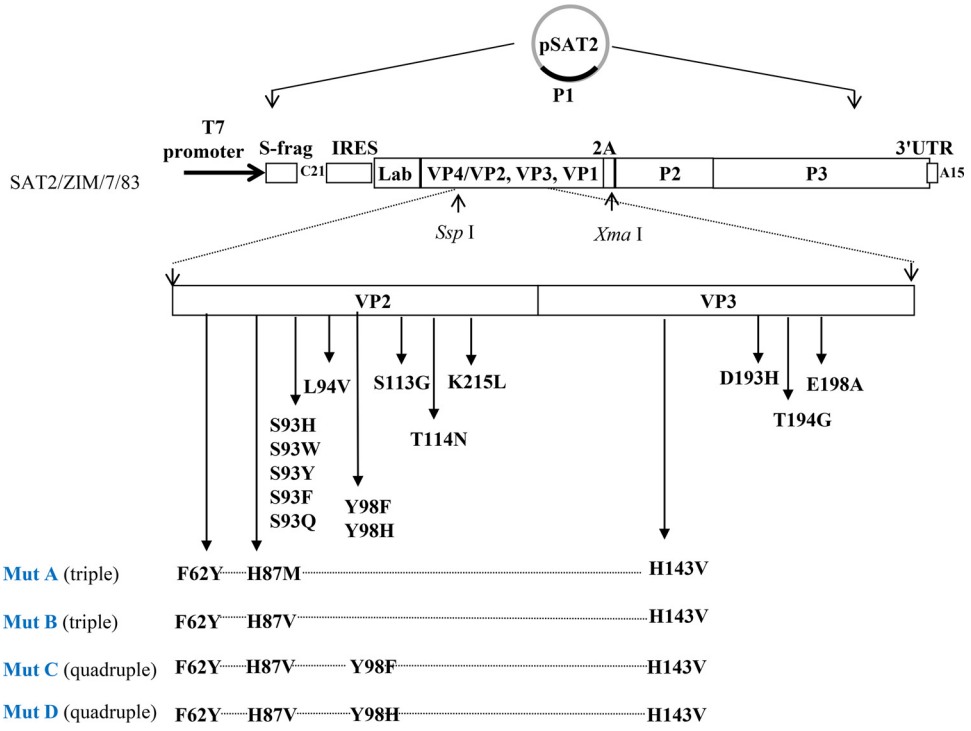

FIG 2 Schematic representation of the mutagenesis strategy used to introduce stabilizing mutations into SAT2/ZIM/7/83. The predicted mutations of the VP2 and VP3 capsid proteins are indicated in single, triple, or quadruple cassettes. The amino acid residues are numbered independently for each protein. In the mutant names, the first digit indicates the protein (VP1, VP2, or VP3) and the last three digits the amino acid position. Following overlap extension mutagenesis, the stabilizing mutated P1 regions were cloned into the SspI and XmaI sites of pSAT2, a genome-length cDNA clone of SAT2/ZIM/7/83. IRES, internal ribosome entry sequence; UTR, untranslated region.

S2093H virus had about a 5-fold increase in virus titer at 24 h compared to that of the WT (Fig. 3). The wild-type, F2062Y-H2087M-H3143V, and S2093H viruses were comparable in their growth kinetics from 0 to 12 h.p.i.

Antigenic profiling of mutant viruses by use of SAT2-specific MAbs. The viable mutant viruses (D3193H, E3198A, S2093H, S2093Y, S2093W, L2094V, and F2062Y-

TABLE 2 Passage histories, plaque morphologies, and titers of SAT2 wild-type and stabilizing mutant viruses

Amino acid change(s)	Passage cell type, plaque morphology	Titer (PFU/ml)[a]
S2093H	BHK, medium/large	1.4×10^7
S2093Y	BHK ZZR, small	1.87×10^5
S2093W	BHK, small/medium	1.00×10^7
S2093Q	BHK, medium/large	7.2×10^3
S2093F	BHK, medium/large	5.2×10^3
L2094V	BHK, medium/large	6.2×10^5
Y2098F	Not viable	ND
Y2098H	Not viable	ND
T2114N	Not viable	ND
S2113G	BHK, medium/large	4.0×10^5
K2215L	Not viable	ND
D3193H	BHK, medium/large	2.2×10^7
T3194A	Not viable	ND
E3198A	BHK, medium/large	4.8×10^5
F2062Y-H2087V-H3143V	BHK, medium/large	6.2×10^3
F2062Y-H2087M-H3143V	BHK, medium/large	8.4×10^7
F2062Y-H2087V-Y2098F-H3143V	Not viable	ND
F2062Y-H2087V-Y2098H-H3143V	Not viable	ND
Wild type	BHK, medium/large	2.0×10^6

[a]ND, not done because the virus was not viable.

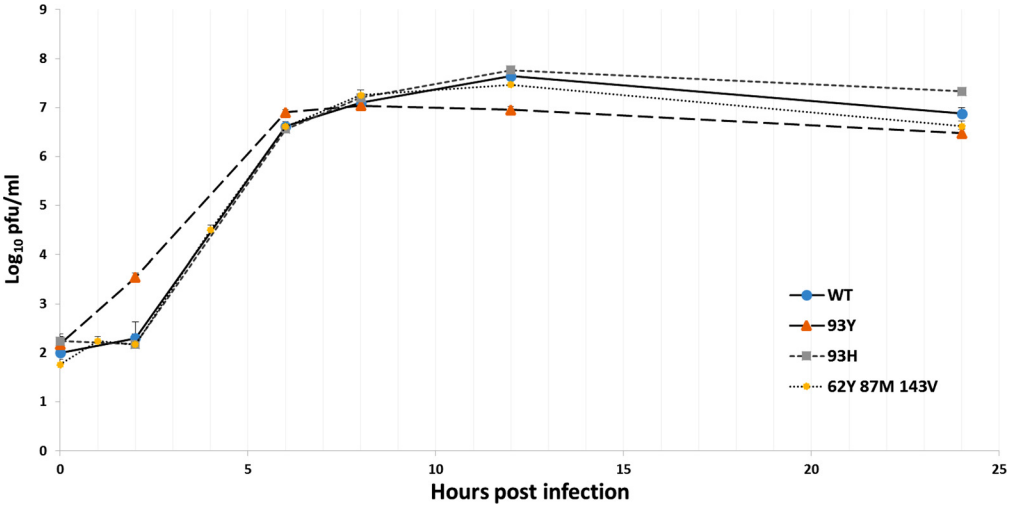

FIG 3 One-step growth kinetics study performed on BHK-21 cells. The average $\log_{10}$ titers for duplicate wells are shown for different time points (0, 1, 2, 4, 6, 8, 12, and 24 h postabsorption), as indicated on the graph, after infection over a 24-h period with the wild-type, S2093H, S2093Y, and F2062Y-H2087M-H3143V mutant viruses. The standard deviations of the titers determined for quadruplicate wells are indicated on the graph.

H2087M-H3143V) and the S2113G virus (negative control) were characterized based on their sandwich enzyme-linked immunosorbent assay (ELISA) absorbance readings in response to SAT2-specific monoclonal antibodies (MAbs). The readings were expressed as ratios of the mutant readings to the readings for the wild-type SAT2 virus. The five MAbs reacted as expected to wild-type vSAT2, as described previously (40). All mutants reacted to DA10, GG1, GE11, and 1D5 similarly to wild-type virus, as shown by similar reactivity profiles (Fig. 4). However, the reactivity of the S2093Y mutant to GD12 was lowered significantly, to 37% ($P < 0.05$), with a ratio profile of 1:4 (S2093Y:wild type) (Fig. 4).

Thermal and acid stabilities of mutants as determined by thermal inactivation assay. The differences in the stabilities of the viruses were elucidated using a thermal inactivation assay. Duplicates of cell culture supernatants containing the wild-type and stability-mutated viruses, with approximate titers of 2×10^5 to 10×10^5 PFU/ml, were either treated at pH 6.0 or heated at 42°C or 49°C for different times of up to 4 h following 1:50 dilution in the appropriate buffer. The number of infectious particles remaining after treatment was determined by plaque titrations on BHK-21 cells. The inactivation of vSAT2 and the mutant viruses at 42°C or 49°C followed linear kinetics, and the inactivation rate values for the mutant viruses were calculated from the slope

Virus / MAb	DA10 :	GG1 :	GE11 :	1D5:	GD12
S2113G (neg)	0.72	0.71	0.76	0.57	1
D3193H	0.806	0.78	0.86	0.68	1
E3198A	0.74	0.7	0.74	0.516	1
S2093H	0.72	0.64	0.69	0.55	1
S2093Y	1	0.91	0.99	0.52	0.25
S2093W	1	0.78	0.96	0.74	0.87
L2094V	1	0.76	0.85	0.7	0.82
F2062Y-H2087M-H3143V	1	0.83	0.81	0.71	0.86
wild-type	**0.83**	**0.74**	**0.87**	**0.65**	**1**

FIG 4 Heat map of the five SAT2-specific MAb (DA10, GG1, GE11, 1D5, and GD12) reactivity ratios for the mutant and wild-type viruses. Absorbance values (averages for three repeats) are shown as the ratio of each MAb's reactivity for the indicated virus. Mock-infected cell supernatants were used as a background control. The ratio depicts a specific profile for each virus. Green shaded areas represent ratio values closest to 1, indicative of the highest reactivity of a given virus to the MAb. Values of <0.5 (orange to red) are indicative of poor reactivity to that MAb and of a result most disparate from the wild-type profile. The binding pattern ratio for the wild-type virus (0.8:0.7:0.9:0.7:1) is used as a control against which mutant virus reactivities can be compared.

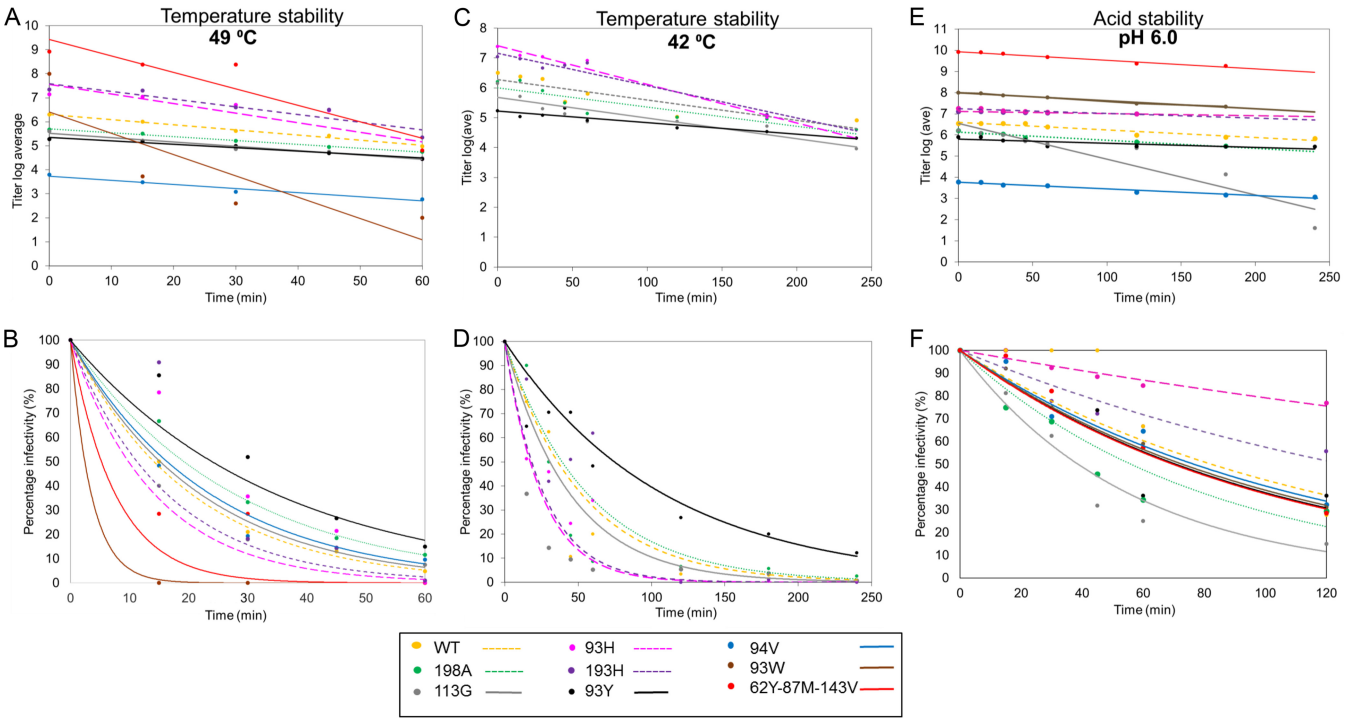

FIG 5 Thermal and pH inactivation kinetics of wild-type and mutant SAT2 viruses tested in duplicate. Inactivation of SDG-purified wild-type and mutant SAT2 particles was determined following heat treatment at 49°C for 1 h (A) or 42°C for 4 h (C) or treatment with TNE buffer at pH 6.0 for 2 h (E). The average $\log_{10}$ virus titers determined for two different inactivation experiments are shown. The respective logarithmic values of the virus titers at the different time points (0, 15, 30, 45, 60, 90, 120, 180, and 240 min postinfection) were linearly fitted and the slopes determined. The average virus titers following heat inactivation at 49°C (B) or 42°C (D) or following pH treatment (F) were used to determine the percentages of residual infectious particles remaining over time.

of the graph (Fig. 5). Lower inactivation rates correlated with increased virus stability. The inactivation rate constants at 49°C for the wild-type, E3198A, L2094V, and S2093Y viruses were 0.022, 0.016, 0.017, and 0.014 min^{-1}, respectively. The percentages of infectious particles remaining after 1 h at 49°C for the S2093Y, E3198A, and L2094V mutants were 15, 12, and 10%, respectively, compared to 5% for the wild-type virus (Fig. 5A and B).

The mutant infectious particles that showed increased thermostability at 49°C were further tested at 42°C for 4 h. The inactivation rate constants at 42°C for the wild-type, E3198A, and S2093Y viruses were 0.007, 0.007, and 0.004 min^{-1}, respectively. Similarly, a lower inactivation rate was observed for the S2093Y infectious particles than for the wild type and the other mutant viruses. The percentages of infectious particles remaining after 1 h at 42°C for the S2093Y and E3198A mutants were 27% and 6.4%, respectively, compared to 3.3% for the wild-type virus, and at 4 h the percentage for the S2093Y mutant was 12%, compared to 2.5% for the wild-type virus (Fig. 5C and D).

The inactivation rate values at room temperature and pH 6.0 showed improved pH stability for the S2093H (0.001 min^{-1}), S2093Y (0.002 min^{-1}), D3193H (0.002 min^{-1}), and E3198A (0.002 min^{-1}) mutant viruses compared to that of the wild-type virus (0.004 min^{-1}); however, the negative-control S2113G mutant (0.017 min^{-1}), which was not selected by *in silico* methods, was considerably less pH stable than the wild type (Fig. 5E and F). The percentages of infectious particles remaining after 2 h of treatment at pH 6.0 for the S2093H, D3193H, and S2093Y mutant viruses were 77%, 56%, and 36%, respectively, with the S2093H mutant having a 28% improvement in pH stability compared to that of the wild type (Fig. 5E and F).

Thermal shift assay of engineered FMDV mutants. Fluorescence thermal shift assays (41) were performed on purified wild-type and mutant SAT2 viruses. Wild-type vSAT2 capsids dissociated at 47°C, whereas most mutants were more thermostable. The S2093Y mutant dissociated at 53.5°C, followed by the E3198A and F2062Y-H2087M-

A

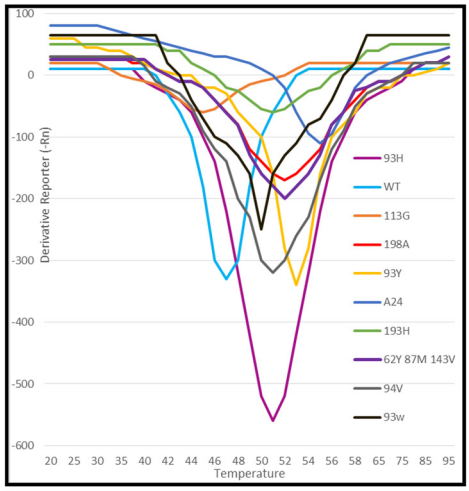

C

virus	control	6.1	6.7	7.2	7.6	8.2	8.5	9.1
Wild-type	47±0.07	37±0	41±0.21	45±0.7	46±0.21	48±0	46±0.14	44±0
93Y	53.5±0.14	36±0	44±0.7	47±0.14	49±0.07	51±0.07	49±0.28	47±0.21
93H	51±0.28	ds*	39±0.28	43±0.21	46±0.28	49±1.4	47±0.21	45±0
93W	50±0	ds*	40±0	45±0.07	49±0.21	51±0	48±0	47±0
94V	51±0	ds*	40±0	45±0.28	48±0	52±0.7	50±0	48±0.35
113G	45±1.9	ds*	34±0.21	36±0.28	41±0	44±0.21	37±0	37±0.28
198A	52±0.21	ds*	41±0	45±0.28	48±0	49±0	47±0	45±0.21
193H	51±0.35	ds*	40±0.21	44±0.21	46±0.35	49±0	44±0	44±0
62Y 87M 143V	52±0.7	ds*	41±0	47±0.07	49±0.14	51±0	48±0.21	ds*
A24	55.5±0.21	38±0.7	43±0.35	50±0.7	50±0.21	52±0.07	50±0.14	49±0.21

B

virus	1M NaCl	0.5M NaCl	1M KCl	0.5M KCl	1M $(NH_4)_2SO_4$	0.5M $(NH_4)_2SO_4$	1M $MgCl_2$	0.5M $MgCl_2$	1M CaCl2	0.5M CaCl2	10% NBS	5% Glycine	VGM	30% sucrose	1xPBS	control
Wild-type	56±0.14	52±0.21	53±0.14	50±0.28	43±0.7	39±0.7	ds*	ds*	45±0.7	48±0.14	48±2.12	53±0.14	51±0.14	47±0.14	54±0.7	47±0.07
93Y	60±1.4	58±0.07	58±1.4	55±1.4	58±1.4	54±0.2	48±0.07	48±0.2	ds*	52±0.2	ds*	49±1.4	56±1.4	59±1.4	57±1.4	53.5±0.14
93H	60±0.21	57±0.28	56±0.07	54±0.21	56±0.28	52±0.7	48±0.14	49±0.21	45±0.7	50±0.7	49±0.21	42±0.7	50±0.28	57±1.4	56±0.14	51±0.28
93W	60±0.21	57±0.21	ds*	53±0.28	56±0.35	52±0.7	ds*	ds*	ds*	ds*	ds*	46±0.7	53±0.21	53±0.14	56±0.42	50±0
94V	ds*	54±0.42	ds*	ds*	52±0.14	50±0.21	ds*	ds*	ds*	ds*	ds*	42±1.14	52±0.14	50±0.70	55±0.28	51±0
113G	58±0.28	54±0.07	50±0.21	48±0.21	51±0.21	48±0.14	43±0.42	42±0.70	45±0.7	48±0.7	ds*	38±0.28	50±0.35	48±2.12	51±0.21	45±1.9
198A	59±0.21	56±0.14	56±0.14	53±0.14	57±0.21	53±0.7	50±0.28	51±0.7	45±0.07	48±0.07	50±0.21	51±0.21	52±0.14	59±0.14	54±0.07	52±0.21
193H	58±0.28	55±0.14	55±0.14	52±0.35	55±0.14	53±0.7	ds*	ds*	44±0.7	47±0.14	ds*	48±0.28	51±0.14	57±0.7	51±0.14	51±0.35
62Y 87M 143V	60±0.21	57±0.14	57±0.14	56±0.07	52±0.7	49±1.4	47±0.28	48±0.07	ds*	ds*	ds*	53±0.14	55±0.14	54±0.7	56±0.21	52±0.7
A24	60±0.07	59±0.11	58±0.14	57±0.21	56±0.07	55±0.07	59±0.21	57±1.4	55±0.21	54±0.21	53±0.07	52±3.53	55±0.7	58±1.4	58±0.07	55.5±0.21

FIG 6 Fluorescence thermal shift assay (41) to determine the dissociation temperatures of the wild-type and mutant SAT2 viruses. The A24 virus was used as a representative control of an A-serotype stable virus. (A) Dissociation temperatures of mutants showing improved temperature stability in comparison to that of controls. (B and C) Heat maps showing average dissociation temperatures of duplicate repeats, with error values. Green shading is indicative of a more stable virus, while red shading shows a more unstable virus. (B) pH stability tested with a range of pH buffers (pH 6.1 to 9.1). (C) Ionic stability of 15 different buffers and their effects as additional improvements to stability. The control was 0.8× PBS. ds*, viruses were dissociated under the experimental conditions, and no reading was obtained.

H3143V mutants (52°C), the L2094V, S2093H, and D3193H mutants (51°C), and the S2093W (50°C) mutant (Fig. 6A). The negative-control S3113G mutant was less stable, with dissociation at 45°C. The A-serotype A24 control virus had the highest temperature stability, with dissociation at 55.5°C (Fig. 6A). The S2093Y mutant had a significantly higher (6°C) capsid stability ($P < 0.05$), while the F2062Y-H2087M-H3143V, E3198A, S2093H, L2094V, and D3193H mutants had 4 to 5°C increases in capsid stability compared to that of the wild-type vSAT2 virus. The more stable A24 control capsid dissociation temperature was only 2°C higher than that of the S2093Y mutant.

Next, we investigated whether elevated temperatures may affect the conformation of the interface by disrupting the secondary/tertiary protein structure permanently or temporarily. The S2093Y mutant and wild-type vSAT2 viruses were heated to 42°C, 49°C, or 53°C for different times of up to 1 h to allow for various degrees of dissociation (partial to full) and then cooled on ice to allow reestablishment of the conformation before performance of the thermal shift stability assay. We found that there was no difference in capsid dissociation temperature for the viruses exposed to different temperatures or times of exposure compared to the normal dissociation temperature (data not shown).

To investigate the effect of pH on capsid stability, sucrose density gradient (SDG)-purified viruses were exposed to buffers in the pH range of 6.1 to 9.1 (Fig. 6C). Sensitivity to pH was measured by the decrease in dissociation temperature compared to that of the phosphate-buffered saline (PBS) control. At pH 6.1, most viruses were fully dissociated, except for the wild-type, S2093Y, and A24 viruses, which were more pH resistant. The viruses were most stable at pH 7.6 to 8.2. The negative-control S2113G mutant was less thermostable and showed greater sensitivity to pH changes.

To investigate the effects of ionic buffers on capsid stability, 16 ionic buffers were examined (Fig. 6B). The following summarizes the trend of the buffers supporting the highest to the lowest stability as assessed by dissociation temperatures: 1 M and 0.5 M NaCl, 1 M KCl, 1 M $(NH_4)_2SO_4$, 1× PBS, 30% sucrose, virus growth medium (VGM), 0.5 M KCl, 0.5 M $(NH_4)_2SO_4$, 5% glycine, 0.5 M $CaCl_2$, 0.5 M and 1 M $MgCl_2$, 1 M $CaCl_2$, and 10% normal bovine serum (NBS).

The 1 M NaCl solution supported the highest increase in stability (except for the L2094V mutant), followed by the 0.5 M NaCl solution, and both of these were significantly different ($P < 0.05$) from the 0.8× PBS control. There was improved stability for all the viruses for 1 M KCl (except for the S2093W and S2094V mutants), VGM, and 1× PBS. The 30% sucrose solution showed improved stability for the S2093Y, S2093H, E3198A, D3193H, and A24 viruses. The 1 M and 0.5 M $MgCl_2$ and $CaCl_2$, 10% NBS, and 5% glycine solutions resulted in the greatest decreases in stability of the SAT2 viruses; however, the A24 control virus was not affected. The wild-type virus was destabilized by the 0.5 and 1 M $(NH_4)_2SO_4$ solutions, whereas the mutant viruses had improved or equivalent stability.

Genetic stability of S2093Y virus upon cytolytic passage in BHK38 suspension cells. To evaluate the relationship between virus stability and virus titer following passage in cultured cells, we subjected the S2093Y mutant virus to six serial amplifications in BHK-21 no. 38 (BHK38; Brescia, Italy) suspension cells and analyzed the progeny populations. Initially, the S2093Y mutant was very slow-growing, but after a few passages it grew faster and had a growth profile, CPE/plaque formation, and end titer in BHK-21 cells similar to those of the parental SAT2/ZIM/7/83 virus. A rapid loss of the mutation during virus replication would suggest some biological disadvantage. An in-depth sequence analysis revealed that the originally introduced TAT (Tyr) codon 93 (VP2) had changed to a CAT (His) codon, while the wild-type AGC codon (Ser) was absent, and no other accompanying mutations were observed in the capsid coding region. This mutation first appeared at passage 3 (33% of the peaks) and was fully preserved at passage 6. Serial passage of the S2093H virus for another 14 cycles did not result in any additional changes, allowing large-scale passage of the engineered virus for vaccine production requirements.

DISCUSSION

To date, experimental studies on the relative importance of residues and molecular interactions in viral capsid assembly, disassembly, and/or stability are limited. Previous attempts at improving stability have had only marginal success (32), while another study reported a stable disulfide bond at the icosahedral 2-fold axis between adjacent pentamers in the A22 virus which allowed the production of thermo- and pH-stable recombinant empty virus-like particles (42). Mateo et al. (43) observed that thermostable variants are not represented among the quasispecies of FMDV serotypes. Hegde et al. (44) therefore speculated that FMDV has evolved to undergo persistency by avoiding establishment of thermostable species. We previously investigated the rational introduction of mutations to increase thermostability by devising a strategy that allows mutations conferring noncovalent stabilization to be evaluated *in silico* (35). In the present study, we investigated a larger panel of amino acid residues, using 14 single amino acid substitutions, 2 triple mutations, and 2 quadruple mutations at the interpentamer interface of the VP2/VP3 capsid proteins of SAT2/ZIM/7/83. The predicted stability mutations were introduced into a full-length SAT2 infectious cDNA clone (pSAT2), and viable mutant viruses were recovered following transfection into BHK-21 cells. We assessed the recombinant mutant virus panel for temperature, pH, and ionic stability, antigenicity to SAT2-specific monoclonal antibodies, growth characteristics, and genetic stability in suspension cells in order to select candidate mutants for engineering stabilized SAT2 vaccines.

The S2093Y and S2093W viruses showed much smaller plaque sizes than that of the wild-type virus. This observation was confirmed by a $\log_{10}$ decrease in the S2093Y mutant titer compared to wild-type virus growth at 12 h.p.i. It is hypothesized that the

increase in stability of the S2093Y mutant contributed to delaying viral genome release (uncoating) and to slower replication of the virus, resulting in a smaller plaque size. O'Donnell et al. (45) found that effective release of the viral genome into the cytoplasm is necessary to begin the replication cycle. Some mutant viruses, such as the quadruple mutants and the S2093F and S2093Q single mutants, were not viable or grew to titers of approximately 3 $\log_{10}$/ml, possibly because of overstabilization leading to poor uncoating and replication. This is in contrast to the findings of Rincón et al. (46), who found that a different strategy of eliminating interpentamer repulsions, by either charge neutralization (A2065H) or charge removal (D2068N, E2086Q, D3134N, or D3195N), resulted in mutants that were nearly as infectious as the nonmutated virus and yielded similar titers in cultured cells.

The S2093Y mutant was scaled up by sequential passages in BHK38 suspension cells and was found to be genetically unstable by acquiring a single nucleotide mutation during passage, resulting in the S2093H mutant. In this study, the S2093H mutant was shown to be less thermostable than the S2093Y mutant but more thermostable than the wild type (93S). Genetic instability may be overcome by species-specific codon optimization in conjunction with the production cell line (47); by the use of stronger base-pairing options at the mutation site and the choice of a cell line which exhibits less reversion (48); by compensatory mutations introduced near the mutation site (49); or by adjusting the MOI, passaging less, improving replication through use of additional ribosome binding sites, or increasing the fidelity of the viral RNA polymerase (49).

The antigenic reactivity of the mutants was assessed to ascertain if the amino acid changes had affected the typical binding of five SAT2 MAbs to the epitopes of the ZIM/7/83 virus as characterized by Opperman et al. (40). The reactivity of the S2093Y mutant to MAb GD12 was lowered to 37% compared to that of the wild type, which is indicative of changes to the GD12 epitope footprint by the S2093Y mutation in VP2. Although we do not have structural data to confirm this, we hypothesize that increased hydrophobic interactions may possibly cause reduced flexibility or local distortion in surface-exposed loops, locking the exposed side chains into a position not optimally aligned to GD12's complementarity-determining regions (CDRs). The exact footprint of GD12 has not yet been mapped, but previous evidence (40) suggests that amino acids at the 2-fold interface form part of the GD12 footprint. The S2093Y mutation is not expected to affect the critical domain for GD12 binding but perhaps to cause imperfect alignment (50–52) of the functional binding region of the capsid and the GD12 CDRs. However, the MAbs tested are nonneutralizing mouse antibodies, and there was no difference in antigenicity of the S2093Y and wild-type antigens when cattle were vaccinated with them (35) or in the duration of immunity at 6 months postvaccination (K. A. Scott, submitted for publication), as well as no apparent difference in the structures of the wild-type and S2093Y capsids (38).

The stabilities of the wild-type and mutant viruses under different temperature, pH, and ionic conditions were assessed using two methods: (i) an inactivation assay measuring infectivity by using live virus particles and (ii) a thermal shift assay (41) measuring capsid dissociation by using purified particles. There was an increase in thermostability compared to that of the wild-type virus for the S2093Y, L2094V, and E3198A mutants by use of the inactivation assay and for the S2093Y, E3198A, F2062Y-H2087M-H3143V, L2094V, S2093H, and D3193H mutants by use of the thermal shift assay. The two assays were comparable, showing a 10-fold increase in thermostability of the S2093Y mutant, similar to that of the stable A24 virus.

Additionally, the stabilities of the mutant viruses under different pH and ionic conditions were evaluated against that of the wild-type virus. The S2093Y, wild-type SAT2, and A24 viruses were more resistant at pH 6.1 than most FMDVs, which are susceptible outside the range of pH 6.0 to 9.0, converting rapidly into pentameric subunits (29–31). The following mutant viruses had improved pH stability compared to that of the wild-type SAT2 virus: the S2093Y mutant, from pH 6.7 to 9.1; the F2062Y-H2087M-H3143V triple mutant, from pH 7.2 to 8.5; and the S2093W and L2094V mutants, from pH 7.6 to 9.1.

The stabilizing effects of different ionic buffers are additive to already introduced stability mutations by neutralizing destabilizing charges on surface-exposed amino acids. Most mutant viruses showed improved stability when exposed to NaCl, $(NH_4)_2SO_4$, and KCl buffers, PBS, 30% sucrose, and VGM. The 1 M NaCl solution resulted in the highest protective effect on the SAT2 capsid, in support of the findings by Kotecha et al. (53). Certain salts, such as 1 M NaCl, are capable of further increasing the thermal stability of these mutant viruses by 6 to 10°C. Protein-protein interactions, such as those mediating subunit assembly and hence capsid stability, are made up of hydrophobic and electrostatic interactions and hydrogen bonds. In the same way that salts can have either a destabilizing effect (chaotropes) or a stabilizing effect (kosmotropes) on protein structures, they can also modulate protein-protein interactions in various ways, depending on the type of salt and its concentration in the buffer environment.

Overall, the most beneficial mutation was in the S2093Y single mutant (for temperature and pH stability), while other promising mutants were the E3198A, L2094V, and S2093H single mutants and the F2062Y-H2087M-H3143V triple mutant. FMDV capsids are held together by weak electrostatic interactions and a series of hydrogen bonds between the pentameric assemblies. We have shown that introducing a single-residue mutation generating hydrophobic stacking of aromatic side chains at the 2-fold axis between adjacent pentamers is effective at stabilizing the particle (35), with little effect on its infectivity. There is a series of histidine residues at the pentameric interfaces, and the protonation of these residues is thought to be responsible for disassembly. Curry et al. (37) and van Vlijmen et al. (54) proposed that VP3 His142 is the trigger for uncoating, and Ellard et al. (31) demonstrated that replacement of this one residue with aspartate renders the capsids stable. Histidine 142 (VP3 position 143 for SAT2) faces the positive end of the alpha-helix dipole located at the 2-fold axis. van Vlijmen et al. (54) reported that the free energy of dissociation contributed by this histidine is attributable to the polarizing effect of the helix dipole. In addition, there is a second conserved histidine, VP2 His87, also located at the positive end of the helix dipole, which might have a similar effect of destabilizing the interface. In enteroviruses, such as enterovirus 71 (EV71) (55), or poliovirus (56), these histidine residues are not present, and there is a tyrosine residue with its OH group pointing to the positive end of the 2-fold helix. Mutating the histidines in FMDV to valines and introducing an additional mutation, F2062Y, stabilized the helix dipole at the positive end and showed an increase in binding free energy in simulation as well as a 5°C increase in thermostability and improved pH stability of the mutant particles compared to the wild-type particles.

The amino acid residues responsible for capsid stabilization in this study, mirrored by *in silico* calculations, have the potential to be used in improving the design of SAT2 vaccines by combining reverse genetic approaches that allow (i) replacement of external capsid coding regions or surface-exposed antigenic regions with those of emergency or more suitable field isolates to transfer improved neutralizing epitopes and (ii) site-directed mutagenesis of amino acids to improve thermostability. Structurally stabilized SAT2 vaccines have a number of advantages in that less strict cold chain logistics are required, especially in Africa, where an absence of a cold chain exists in remote regions, and they have an improved duration of immunity due to less degradation (35). Previously we reported that formulated vaccines from inactivated wild-type and stabilized S2093Y SAT2 viruses produced equivalent protective levels of neutralizing antibodies in cattle for 35 days; in addition, after storage for 1 or 6 months at 4°C, S2093Y particles produced substantially higher neutralizing antibodies in guinea pigs than those induced by wild-type particles, corresponding to shelf-life improvement (35). Future work will be performed to assess the differences in cellular and humoral immune responses, shelf-life, and potency between wild-type and stabilized S2093Y and S2093H antigens in cattle.

MATERIALS AND METHODS

Cells, viruses, and plasmids. Baby hamster kidney (BHK) clone 13 cells (strain 21; ATCC CCL-10) were maintained and propagated in Eagle's basal medium (BME; Life Technologies). RNA transfection, virus

passage, and virus stocks were prepared or performed with BHK-21 cells (57) by using virus growth medium (VGM; BME with 1% [vol/vol] fetal calf serum [FCS], 1% [vol/vol] HEPES, and antibiotics). The plasmid pSAT2, a previously described genome-length infectious cDNA clone of SAT2/ZIM/7/83 (38), was used as the genetic backbone for the construction of recombinant cDNA clones harboring capsid-stabilizing mutations. The virus recovered from pSAT2 is referred to as vSAT2. BHK38 (Brescia, Italy) suspension cells were used to scale up the S2093Y mutant for vaccine production by using virus growth medium (VGM; enriched minimum essential medium [MEM] with 1% [vol/vol] normal bovine serum [NBS]).

Identification of stabilizing residues. Model preparation for molecular dynamics simulations, the design and construction of candidate mutants, the molecular dynamics simulation protocol, and estimation of the degree of stabilization for SAT2/ZIM7/83 have previously been described in detail (35). Briefly, a dimeric interpentamer interface was generated from the atomic model of SAT1 (36) (PDB ID 2WZR) and used as a starting template. A truncated model which contained all atoms within 13 Å of an interface was then generated and simulated for 1.55 ns, with an explicit solvent model using AMBER10 (58). A set of restraints were introduced by placing dummy atoms along the interface, and all atoms outside a 10-Å radius from the dummy atoms were heavily restrained, as were the dummy atoms themselves (35). A binding free energy between adjacent protomers (from different pentamers) was calculated using the molecular mechanics Poisson-Boltzmann (MM-PBSA) method (59). Finally, the difference in binding free energy, $\Delta\Delta G$, between candidate mutant models and the parent wild-type model was calculated to assess the stability of the mutants.

Generation of recombinant SAT2 cDNA mutants. The ca. 2.2-kb external capsid coding region (1B-1D/2A) of the plasmid pSAT2 (38) was digested with the endonucleases EcoRI and XmaI and cloned into corresponding sites of the pBluescript II SK (pBS; Stratagene) vector to generate the template for site-directed mutagenesis (pBS-P1). The S2093H, S2093Y, and S2093W mutants were described previously (35), but more in-depth analyses were performed on them in this study. Mutations were introduced into pBS-P1 (120 ng) by use of overlapping inner mutagenesis oligonucleotides and a QuikChange site-directed mutagenesis kit (Stratagene) according to the manufacturer's instructions. Cycling conditions were as follows: 95°C followed by 18 cycles of 95°C for 30 s, 55°C for 60 s, and 68°C for 6 min.

The mutated pBS-P1 constructs were confirmed by sequencing (BigDye Terminator v3.1 cycle sequencing kit; Applied Biosystems). The mutated external capsid coding region (1B-1D/2A) of plasmid pBS-P1 was digested with the endonucleases SspI and XmaI to recover the mutated capsid coding region and cloned back into pSAT2. The mutated recombinant pSAT2 constructs were confirmed by nucleotide sequencing.

***In vitro* RNA synthesis and transfection and virus recovery.** Recombinant, mutated pSAT2 plasmids were linearized with SwaI and *in vitro* transcribed using a MEGAscript T7 kit (Ambion). The integrity of the RNA was analyzed by agarose gel electrophoresis. *In vitro*-transcribed RNA (3 μg) was transfected into BHK-21 cells by use of Lipofectamine 2000 reagent (Life Technologies) according to the manufacturer's instructions. Transfected cells were maintained at 37°C with a 5% CO_2 influx for 48 h in virus growth medium and frozen at −80°C. Viruses (termed "passage 0" [P0]) were subsequently harvested from infected cells by a freeze-thaw cycle and clarified by centrifugation. Fetal goat tongue (ZZ-R CCLV-RIE127) (39) or BHK-21 cells were subsequently used to passage the viruses up to six times or until >90% CPE was observed. The mutated viruses derived from the genome-length cDNA (Fig. 2) were confirmed by nucleotide sequencing and used in subsequent experiments.

Sequence confirmation of mutant recombinant viruses. Total RNA was extracted from infected cell cultures by use of a QIAamp viral RNA minikit (Qiagen) according to the manufacturer's specifications and then used as the template for cDNA synthesis. Viral cDNA was synthesized with SuperScript III (Life Technologies) and the oligonucleotide 2B208R (5′-GACATGTCCTCCTGCATGTG) (60) at 50°C for 50 min. The leader/capsid coding region of the mutated viruses was amplified using Expand long-template *Taq* DNA polymerase (Roche) with genome-specific oligonucleotides (NCR2 [5′-GCTTCTATGCCTGAATAGG] and WDA [5′-GAAGGGCCCAGGGTTGGACTC]). Direct DNA sequencing of the amplicons or plasmids was performed using an ABI PRISM BigDye Terminator cycle sequencing ready reaction kit v3.0 (PerkinElmer Applied Biosystems). The consensus nucleotide sequence of the capsid coding region was assembled with Sequencher 4.7 DNA sequence analysis software (Gene Codes Corporation) and compared to that of SAT2/ZIM/7/83 (GenBank accession no. JQ639289 and DQ009726).

Plaque, growth kinetics, and thermal inactivation assays. Plaque assays were performed in triplicate by infecting BHK-21 monolayer cells in 35-mm cell culture plates (Nunc) for 1 h, followed by the addition of a 2-ml tragacanth overlay (57). Following incubation at 37°C for 48 h, the infected monolayers were stained with 1% (wt/vol) methylene blue in 10% (vol/vol) ethanol and 10% (vol/vol) formaldehyde in phosphate-buffered saline, pH 7.4. The diameters of >50 parental (wild-type) plaques were measured with a microscope eyepiece micrometer. These were averaged, defined as 100%, and compared against >50 mutant plaque diameters.

One-step growth kinetics analyses were performed by infecting BHK-21 cell monolayers with the wild-type and S2093H, S2093Y, and F2062Y-H2087M-H3143V mutant viruses at MOIs of 3 to 5. After 1 h of adsorption, cells were washed with MBS (MES-buffered saline; 25 mM morpholineethanesulfonic acid [MES], 145 mM NaCl, pH 5.5) and then incubated with VGM at 37°C. At 0, 1, 4, 6, 8, 12, and 24 h.p.i., infected cells were frozen at −80°C. Virus titers were determined by plaque assays and expressed in PFU per milliliter as described above.

Thermal inactivation was performed on wild-type and mutant viruses in cell culture supernatants diluted in TNE buffer (100 mM Tris, pH 7.4, 10 mM EDTA, 150 mM NaCl) essentially as described previously (61). Briefly, 2×10^5 to 5×10^5 PFU/ml of infectious particles was incubated in duplicate at temperatures

of 42°C and 49°C for 0, 15, 30, 45, 60, 120, 180, and 240 min. Following cooling on ice, the viruses were titrated on BHK-21 cells. Similarly, a pH inactivation kinetics assay was performed in TNE buffer with a pH of 6.0 and a constant temperature (25°C) for the same times as those described above. The samples were subsequently neutralized with 1 M Tris (pH 7.4)-150 mM NaCl and titrated on BHK-21 cells. The respective logarithmic values of the virus titers at the different time points were linearly fitted, and the slopes were determined (43, 62). The percentage of remaining infectious particles was also calculated and plotted, along with the exponential decline, used to calculate the inactivation rate constant (28). The percentage of remaining PFU was determined as the last titer (4 h) divided by the initial titer (0 min) × 100.

Virus purification. Infected BHK-21 cell monolayers were lysed with 0.1% (wt/vol) Nonidet and 20 mM EDTA (pH 8.0) and clarified by centrifugation at 2,000 × *g* for 30 min at 4°C. Virus in the supernatant was inactivated with 5 mM binary ethyleneimine (BEI) for 26 h at 26°C and concentrated using 8% polyethylene glycol 8000 (PEG 8000; Sigma-Aldrich) prior to being purified on 10 to 50% (wt/vol) sucrose density gradients (SDG) prepared in TNE buffer (50 mM Tris [pH 7.4], 10 mM EDTA, 150 mM NaCl) (61). Following fractionation, peak fractions corresponding to 146S virion particles were calculated using an extinction coefficient (E_{259}) of 79.9 (63) and pooled for analysis. Complete inactivation was verified by titration on BHK-21 cells.

PaSTRY. The particle stability thermal release assay (PaSTRY) (41) was performed in 96-well PCR plates by use of an ABI 7500 PCR machine. All assays were performed using 300 to 500 ng of virus and 5 μl of 100× SYBR green II dye (diluted 1:100; Molecular Probes, Invitrogen), with the volume made up to 50 μl with 1× PBS. The temperature was ramped from 15°C to 95°C in 0.5°C increments with intervals of 10 s. SYBR green II fluorescence was read with excitation and emission wavelengths of 490 nm and 516 nm, respectively. The release of RNA, and hence the dissociation of capsids, was detected by an increase in the fluorescence signal, and the melting temperature was taken as the minimum of the negative first derivative of the fluorescence curve. The A-serotype A24 Cruzeiro virus (64) is very thermostable and was used as a positive control in the thermal shift assays.

The ionic buffers (at the indicated final concentrations) tested were 1 M and 0.5 M NaCl, KCl, $(NH_4)_2SO_4$, $MgCl_2$, and $CaCl_2$, 10% NBS, 5% glycine, VGM, 30% sucrose, and 0.8× (control reaction) and 1× PBS, using SYBR green II dye and the virus concentrations described above. The pH buffers were composed of MBS (MES-buffered saline; pH 6.1, 6.7, 7.2, 7.6, 8.2, 8.5, and 9.1).

Alternatively, SDG-purified wild-type virus and the S2093Y mutant virus (500 ng) were made up to 45 μl with 1× PBS, exposed to 42°C, 49°C, and 53°C for 0, 15, 30, 45, and 60 min, and then placed on ice. Five-microliter aliquots of 100× SYBR green II dye were added to samples and a particle stability thermal release assay performed as described above.

Scale-up production of S2093Y mutant in BHK-21 suspension cells. The S2093Y mutant virus was serially passaged in BHK38 (Brescia, Italy) suspension cells up to six times. During the scale-up process, the growth profile, antigenicity, and end titers were determined as described above. At each passage, the P1 region of the S2093Y mutant virus was sequenced and the deduced amino acid sequence compared to that of the wild type.

Sandwich antibody ELISA with SAT2-specific MAbs. Five nonneutralizing, SAT2-specific MAbs (mouse IgG1 isotype MAbs 1D5 [14 μg/ml], DA10 [8 μg/ml], GE11 [19 μg/ml], GD12 [15 μg/ml], and GG1 [22 μg/ml]) have been described elsewhere (40). The MAbs, prepared by inoculating mice with purified 146S antigens (40), were found by mutational analysis of the virus to interact with either (i) two sites on the VP2 protein, i.e., residues 71 and 72 and residues 133 and 134, or (ii) a site that spans the 2-fold axis and involves residues on VP2 and VP3 (40).

A sandwich ELISA was used to titrate the five MAbs and to characterize the wild-type ZIM7/83 virus (40) and nine stabilizing mutant viruses (purified or cell supernatant) and was repeated three times. Equivalent amounts of purified virus or PFU were used. Maxisorp ELISA plates (Nunc) were coated with an optimal dilution of rabbit SAT2 antiserum (SAT2/ZIM/7/83) in 50 mM carbonate-bicarbonate buffer (pH 9.6) and stored overnight at 4°C. Serial 2-fold dilution series (1:5 to 1:40) of the wild-type ZIM7/83 virus and nine mutant viruses (cell supernatant or purified) in blocking buffer (0.05 M Tris, 0.15 M KCl containing 0.5% [wt/vol] milk powder) were applied to the ELISA plates. Viruses were trapped by incubation at 37°C for 1 h, after which the plates were washed with 1× PBS containing 0.05% (vol/vol) Tween 20 (PBS-0.05%T). Twofold dilutions (1:20 to 1:80) of each of the MAbs, prepared in blocking buffer, were added and the plates incubated at 37°C for 1 h. The ELISA plates were washed with PBS-0.05%T, and horseradish peroxidase (HRP)-conjugated rabbit anti-mouse IgG (Sigma-Aldrich), diluted 1:20,000 in blocking buffer, was added. Following incubation at 37°C for 1 h and washing, the ELISA plates were developed. The binding of the MAbs to the viruses was calculated as follows. The mean absorbance reading at 450 nm (A_{450}) for the binding of each MAb to the viruses was corrected by subtracting the background value. The adjusted A_{450} value for each MAb and the mutant viruses was then expressed as a percentage of the mean A_{450} value obtained with vSAT2.

Data analysis. Statistical analyses were performed using one-way analysis of variance (ANOVA) (followed by Dunnett's multiple-comparison test with the control) or the *t* test. The confidence interval was 95%. Statistical analyses were carried out using GraphPad Prism v5.0 (GraphPad Software).

ACKNOWLEDGMENTS

We are grateful to the Wellcome Trust for a Translation Award to fund this work (grant 089755 to B.C., E.E.F., and F.F.M.). The work of the Wellcome Trust Centre in Oxford is supported by Wellcome Trust core award 090532/Z/09/Z. B.C. and D.I.S. are supported as Jenner investigators, J.R. and A.K. are supported by the Wellcome Trust,

and E.E.F. and D.I.S. are supported by the UK MRC (grants G100099 and MR/N00065X/1 to D.I.S.).

We are grateful to the novel vaccine staff and the production team at ARC-OVI for technical assistance. We thank Danny Goovaerts, Elizabeth Rieder, and R. M. Esnouf for helpful discussions.

REFERENCES

1. Mateu MG, da Silva JL, Rocha E, de Brum DL, Alonso A, Enjuanes L, Domingo E, Barahona H. 1988. Extensive antigenic heterogeneity of foot-and-mouth disease virus of serotype C. Virology 167:113–124. https://doi.org/10.1016/0042-6822(88)90060-8.
2. Martínez MA, Dopazo J, Hernández J, Mateu MG, Sobrino F, Domingo E, Knowles NJ. 1992. Evolution of the capsid protein genes of foot-and-mouth disease virus. Antigenic variation without accumulation of amino acid substitutions over six decades. J Virol 66:3557–3565.
3. Domingo E, Diez J, Martinez MA, Hernandez JH, Holguin A, Borrego B, Mateu MG. 1993. New observations on antigenic diversification of RNA viruses. Antigenic variation is not dependent on immune selection. J Gen Virol 74:2039–2045.
4. Knight-Jones TJ, Rushton J. 2013. The economic impacts of foot and mouth disease—what are they, how big are they and where do they occur? Prev Vet Med 112:161–173. https://doi.org/10.1016/j.prevetmed.2013.07.013.
5. Scoones I, Bishi A, Mapitse N, Moerane R, Penrith ML, Sibanda R, Thomson G, Wolmer W. 2010. Foot-and-mouth disease and market access: challenges for the beef industry in southern Africa. Development 1:135–164.
6. Perry BD, Randolph TF. 2003. The economics of foot-and-mouth disease, its control and its eradication, p 23–41. *In* Dodet B, Vicari M (ed), Foot-and-mouth disease: control strategies. Éditions scientifiques et médicales. Elsevier SAS, France.
7. Rweyemamu M, Roeder P, Mackay D, Sumption K, Brownlie J, Leforban Y, Valarcher JF, Knowles NJ, Saraiva V. 2008. Epidemiological patterns of foot-and-mouth disease worldwide. Transbound Emerg Dis 55:57–72. https://doi.org/10.1111/j.1865-1682.2007.01013.x.
8. Hedger RS. 1972. Foot-and-mouth disease and the African buffalo (*Syncerus caffer*). J Comp Pathol 82:19–28. https://doi.org/10.1016/0021-9975(72)90022-9.
9. Hedger RS, Condy JB, Golding SM. 1972. Infection of some species of African wildlife with foot-and-mouth disease virus. J Comp Pathol 82:455–461. https://doi.org/10.1016/0021-9975(72)90045-X.
10. Bengis RG, Kock RA, Fischer J. 2002. Infectious animal diseases: the wildlife/livestock interface. Rev Sci Tech 21:53–65.
11. Thomson GR, Vosloo W, Bastos AD. 2003. Foot and mouth disease in wildlife. Virus Res 91:145–161. https://doi.org/10.1016/S0168-1702(02)00263-0.
12. Vosloo W, Bastos AD, Kirkbride E, Bengis RG, Keet DF, Thomson G. 1996. Persistent infection of African buffalo (*Syncerus caffer*) with SAT-type foot-and-mouth disease viruses: rate of fixation of mutations, antigenic change and interspecies transmission. J Gen Virol 77:1457–1467. https://doi.org/10.1099/0022-1317-77-7-1457.
13. Vosloo W, Bastos AD, Sangare O, Hargreaves SK, Thomson GR. 2002. Review of the status and control of foot-and-mouth disease in sub-Saharan Africa. Rev Sci Tech 21:437–449.
14. Ayebazibwe C, Mwiine FN, Tjornehoj K, Balinda SN, Muwanika VB, Ademun Okurut AR, Belsham GJ, Norman P, Siegismund HR, Alexandersen S. 2010. The role of African buffalos (*Syncerus caffer*) in the maintenance of foot-and-mouth disease in Uganda. BMC Vet Res 6:54. https://doi.org/10.1186/1746-6148-6-54.
15. Dawe PS, Flanagan FO, Madekurozwa RL, Sorensen KJ, Anderson EC, Foggin CM, Ferris NP, Knowles NJ. 1994. Natural transmission of foot-and-mouth disease virus from African buffalo (*Syncerus caffer*) to cattle in a wildlife area of Zimbabwe. Vet Rec 134:230–232. https://doi.org/10.1136/vr.134.10.230.
16. Thomson GR. 1994. Foot-and-mouth disease, p 825–852. *In* Coetzer JAW, Thomson GR, Tustin RC (ed), Foot-and-mouth disease. Oxford University Press, Cape Town, South Africa.
17. Bastos AD, Boshoff CI, Keet DF, Bengis RG, Thomson GR. 2000. Natural transmission of foot-and-mouth disease virus between African buffalo (*Syncerus caffer*) and impala (*Aepyceros melampus*) in the Kruger National Park, South Africa. Epidemiol Infect 124:591–598. https://doi.org/10.1017/S0950268899004008.
18. Vosloo W, Thomson GR. 2004. Natural habitats in which foot-and-mouth disease viruses are maintained, p 384–410. *In* Domingo E, Sobrino F (ed), Foot-and-mouth disease: current perspectives. Horizon Bioscience, Norfolk, United Kingdom.
19. Jori F, Caron A, Thompson PN, Dwarka R, Foggin C, de Garine-Wichatitsky M, Hofmeyr M, van Heerden J, Heath L. 2014. Characteristics of foot-and-mouth disease viral strains circulating at the wildlife/livestock interface of the Great Limpopo Transfrontier conservation area. Transbound Emerg Dis 63:e58–e70. https://doi.org/10.1111/tbed.12231.
20. Ahmed HA, Salem SA, Habashi AR, Arafa AA, Aggour MGA, Salem GH, Gaber AS, Selem O, Abdelkader SH, Knowles NJ, Madi M, Valdazo-González B, Wadsworth J, Hutchings GH, Mioulet V, Hammond JM, King DP. 2012. Emergence of foot-and-mouth disease virus SAT2 in Egypt during 2012. Transbound Emerg Dis 59:476–481. https://doi.org/10.1111/tbed.12015.
21. Chardonnet P, des Clers B, Fischer J, Gerhold R, Jori F, Lamarque F. 2002. The value of wildlife. Rev Sci Tech 21:15–51.
22. Brückner GK, Vosloo W, Du Plessis BJ, Kloeck PE, Connoway L, Ekron MD, Weaver DB, Dickason CJ, Schreuder FJ, Marais T, Mogajane ME. 2002. Foot-and-mouth disease: the experience of South Africa. Rev Sci Tech 21:751–776.
23. Doel TR, Baccarini PJ. 1981. Thermal stability of foot-and-mouth disease virus. Arch Virol 70:21–32. https://doi.org/10.1007/BF01320790.
24. Rossmann MG, Johnson JE. 1989. Icosahedral RNA virus structure. Annu Rev Biochem 58:533–573.
25. Fry E, Logan D, Acharya R, Fox G, Rowlands D, Brow R, Stuart D. 1990. Architecture and topography of an aphthovirus. Semin Virol 1:439–451.
26. Reguera J, Carreura A, Roilobos L, Almendral JM, Mateu MG. 2004. Role of interfacial amino acid residues in assembly, stability, and conformation of a spherical virus capsid. Proc Natl Acad Sci U S A 101:2724–2729. https://doi.org/10.1073/pnas.0307748101.
27. Reguera J, Grueso E, Carreira A, Sánchez-Martínez C, Almendral JM. 2005. Functional relevance of amino acid residues involved in interactions with ordered nucleic acid in a spherical virus. J Biol Chem 280:17969–17977. https://doi.org/10.1074/jbc.M500867200.
28. Mateo R, Diaz A, Baranowski E, Mateu MG. 2003. Complete alanine scanning of intersubunit interfaces in a foot-and-mouth disease virus capsid reveals critical contributions of many side chains to particle stability and viral function. J Biol Chem 278:41019–41027. https://doi.org/10.1074/jbc.M304990200.
29. Acharya R, Fry E, Stuart D, Fox G, Rowlands D, Brown F. 1989. The three-dimensional structure of foot-and-mouth disease virus at 2.9 A resolution. Nature 337:709–716. https://doi.org/10.1038/337709a0.
30. Curry S, Fry E, Blakemore W, Abu-Ghazaleh R, Jackson T. 1996. Perturbations in the surface structure of A22 Iraq foot-and-mouth disease virus accompanying coupled changes in host cell specificity and antigenicity. Structure 4:135–145. https://doi.org/10.1016/S0969-2126(96)00017-2.
31. Ellard FM, Drew J, Blakemore WE, Stuart DI, King AM. 1999. Evidence for the role of His-142 of protein 1C in the acid-induced disassembly of foot-and-mouth disease virus capsids. J Gen Virol 80:1911–1918. https://doi.org/10.1099/0022-1317-80-8-1911.
32. Mateo R, Luna E, Rincon V, Mateu MG. 2008. Engineering viable foot-and-mouth disease viruses with increased thermostability as a step in the development of improved vaccines. J Virol 82:12232–12240. https://doi.org/10.1128/JVI.01553-08.
33. Maree FF, Kasanga CJ, Scott KA, Opperman PA, Chitray M, Sangula A, Sallu R, Sinkala Y, Wambura P, King DP, Paton D, Rweyamamu MM. 2014. Challenges and prospects for the control of foot-and-mouth disease: an African perspective. J Vet Med Res Rep 5:119–138.
34. Doel TR, Chong WKT. 1982. Comparative immunogenicity of 146S, 75S

and 12S particles of foot-and-mouth disease virus. Arch Virol 73: 185–191. https://doi.org/10.1007/BF01314726.
35. Kotecha A, Seago J, Scott K, Burman A, Loureiro S, Ren J, Porta C, Ginn HM, Jackson T, Perez-Martin E, Siebert CA, Paul G, Huiskonen JT, Jones IM, Esnouf RM, Fry EE, Maree FF, Charleston B, Stuart DI. 2015. Structure-based energetics of protein interfaces guides foot-and-mouth disease virus vaccine design. Nat Struct Mol Biol 22:788–794. https://doi.org/10.1038/nsmb.3096.
36. Reeve R, Blignaut B, Esterhuysen JJ, Opperman P, Matthews L, Fry EE, de Beer TAP, Theron J, Rieder E, Vosloo W, O'Neill HG, Haydon DT, Maree FF. 2010. Sequence-based prediction for vaccine strain selection and identification of antigenic variability in foot-and-mouth disease virus. PLoS Comput Biol 6:e1001027. https://doi.org/10.1371/journal.pcbi.1001027.
37. Curry S, Abrams CC, Fry E, Crowther JC, Belsham GJ, Stuart DI, King AMQ. 1995. Viral RNA modulates the acid sensitivity of foot-and-mouth disease virus capsids. J Virol 69:430–438.
38. Van Rensburg HG, Henry T, Mason PW. 2004. Studies of genetically defined chimeras of a European type A virus and a South African Territories type 2 virus reveal growth determinants for foot-and-mouth disease virus. J Gen Virol 85:61–68. https://doi.org/10.1099/vir.0.19509-0.
39. Brehm KE, Ferris NP, Lenk M, Riebe R, Haas B. 2009. Highly sensitive fetal goat tongue cell line for detection and isolation of foot-and-mouth disease virus. J Clin Microbiol 47:3156–3160. https://doi.org/10.1128/JCM.00510-09.
40. Opperman PA, Rotherham LS, Esterhuyzen J, Charleston B, Juleff N, Capozzo AV, Theron J, Maree FF. 2014. Determining the epitope dominance on the capsid of a serotype SAT2 foot-and-mouth disease virus by mutational analyses. J Virol 88:8307–8318. https://doi.org/10.1128/JVI.00470-14.
41. Walter TS, Renm J, Tuthill TJ, Rowlands DJ, Stuart DI, Fry EE. 2012. A plate-based high throughput assay for virus stability and vaccine formulation. J Virol Methods 185:166–170. https://doi.org/10.1016/j.jviromet.2012.06.014.
42. Porta C, Kotecha A, Burman A, Jackson T, Ren J, Loureiro S, Jones IM, Fry EE, Stuart DI, Charleston B. 2013. Rational engineering of recombinant picornavirus capsids to produce safe, protective vaccine antigen. PLoS Pathog 9:e1003255. https://doi.org/10.1371/journal.ppat.1003255.
43. Mateo R, Luna E, Mateu MG. 2007. Thermostable variants are not generally represented in foot-and-mouth disease virus quasispecies. J Gen Virol 88:859–864. https://doi.org/10.1099/vir.0.82521-0.
44. Hegde NR, Maddur MS, Rao PP, Kaveri SV, Bayry J. 2009. Thermostable foot-and-mouth disease virus as a vaccine candidate for endemic countries: a perspective. Vaccine 27:2199–2201. https://doi.org/10.1016/j.vaccine.2009.01.032.
45. O'Donnell V, La Rocco M, Duque H, Baxt B. 2005. Analysis of foot-and-mouth disease virus internalization events in cultured cells. J Virol 79:8506–8518. https://doi.org/10.1128/JVI.79.13.8506-8518.2005.
46. Rincón V, Rodriguez-Huete A, Lopez-Arguello S, Ibarra-Molero B, Sanchez-Ruiz JM, Harmsen MM, Mateu MG. 2014. Identification of the structural basis of thermal lability of a virus provides a rationale for improved vaccines. Structure 22:1560–1570. https://doi.org/10.1016/j.str.2014.08.019.
47. Zhou JH, Zhang J, Chen HT, Ma LN, Ding YZ, Peisak Z, Liu YS. 2011. The codon usage model of the context flanking each cleavage site in the polyprotein of foot-and-mouth disease virus. Infect Genet Evol 11: 1815–1819. https://doi.org/10.1016/j.meegid.2011.07.014.
48. Macadam AJ, Ferguson G, Stone DM, Meredith J, Knowlson S, Auda G, Almond JW, Minor PD. 2006. Rational design of genetically stable live-attenuated poliovirus vaccines of all three serotypes: relevance to poliomyelitis eradication. J Virol 80:8653–8663. https://doi.org/10.1128/JVI.00370-06.
49. Luongo C, Winter CC, Collins PL, Buchholz UJ. 2012. Increased genetic and phenotypic stability of a promising live-attenuated respiratory syncytial virus vaccine candidate by reverse genetics. J Virol 86: 10792–10804. https://doi.org/10.1128/JVI.01227-12.
50. Colman PM, Varghese JN, Laver WG. 1983. Structure of the catalytic and antigenic sites in influenza virus neuraminidase. Nature 303:41–44. https://doi.org/10.1038/303041a0.
51. Colman PM. 1997. Virus versus antibody. Structure 5:591–593. https://doi.org/10.1016/S0969-2126(97)00214-1.
52. Lin G, Nara PL. 2007. Designing immunogens to elicit broadly neutralizing antibodies to the HIV-1 envelope glycoprotein. Curr HIV Res 5:514–541. https://doi.org/10.2174/157016207782418489.
53. Kotecha A, Zhang F, Juleff N, Jackson T, Perez E, Stuart D, Fry E, Charleston B, Seago J. 2016. Application of the Thermofluor PaSTRy technique for improving foot-and-mouth disease virus vaccine formulation. J Gen Virol 97:1557–1565. https://doi.org/10.1099/jgv.0.000462.
54. van Vlijmen HWT, Curry S, Schaefer M, Karplus M. 1998. Titration calculations of foot-and-mouth disease virus capsid and their stabilities as a function of pH. J Mol Biol 275:295–308. https://doi.org/10.1006/jmbi.1997.1418.
55. Wang X, Peng W, Ren J, Hu Z, Jiwei X, Lou Z, Li X, Yin W, Shen X, Porta C. 2012. A sensor-adaptor mechanism for enterovirus uncoating from structures of EV71. Nat Struct Mol Biol 19:424–429. https://doi.org/10.1038/nsmb.2255.
56. Basavappa R, Syed R, Flore O, Icenogle JP, Filman DJ, Hogle JM. 1994. Role and mechanism of the maturation cleavage of VP0 in poliovirus assembly: structure of the empty capsid assembly intermediate at 2.9 A resolution. Protein Sci 3:1651–1669. https://doi.org/10.1002/pro.5560031005.
57. Rieder E, Bunch T, Brown F, Mason PW. 1993. Genetically engineered foot-and-mouth disease viruses with poly(C) tracts of two nucleotides are virulent in mice. J Virol 67:5139–5145.
58. Case DA, Cheatham TE, Darden T, Gohlke DT, Luo R, Merz KM. 2005. The Amber biomolecular simulation programs. J Comput Chem 26: 1668–1688. https://doi.org/10.1002/jcc.20290.
59. Kollman PA, Massova I, Reyes C, Kuhn B, Huo S, Chong L, Lee M, Lee T, Duan Y, Wang W. 2000. Calculating structures and free energies of complex molecules: combining molecular mechanics and continuum models. Acc Chem Res 33:889–897. https://doi.org/10.1021/ar000033j.
60. Bastos AD, Haydon DT, Forsberg R, Knowles NJ, Anderson EC, Bengis RG, Nel LH, Thomson GR. 2001. Genetic heterogeneity of SAT-1 type foot-and-mouth disease viruses in southern Africa. Arch Virol 146:1537–1551. https://doi.org/10.1007/s007050170077.
61. Knipe T, Rieder E, Baxt B, Ward G, Mason PW. 1997. Characterization of synthetic foot-and-mouth disease virus provirions separates acid-mediated disassembly from infectivity. J Virol 71:2851–2856.
62. Mateo R, Mateu MG. 2007. Deterministic, compensatory mutational events in the capsid of foot-and-mouth disease virus in response to the introduction of mutations found in viruses from persistent infections. J Virol 81:1879–1887. https://doi.org/10.1128/JVI.01899-06.
63. Doel TR, Mowat GN. 1985. An international collaborative study on foot and mouth disease virus assay methods. 2. Quantification of 146S particles. J Biol Stand 13:335–344. https://doi.org/10.1016/S0092-1157(85)80048-2.
64. Moraes MP, Mayr GA, Mason PW, Grubman MJ. 2002. Early protection against homologous challenge after a single dose of replication-defective human adenovirus type 5 expressing capsid proteins of foot-and-mouth disease virus (FMDV) strain A24. Vaccine 20:1631–1639. https://doi.org/10.1016/S0264-410X(01)00483-2.